Dynamic Object Tracking Control for a Non-Holonomic Wheeled Autonomous Robot

Yin-Tien Wang[1]*, Yu-Cheng Chen[1] and Ming-Chun Lin[2]

[1]*Department of Mechanical and Electro-Mechanical Engineering, Tamkang University, Tamsui, Taiwan 251, R.O.C.*
[2]*Department of Electrical Engineering, Technology and Science Institute of Northern Taiwan, Taipei, Taiwan, R.O.C.*

Abstract

This paper is devoted to design and implement a non-holonomic wheeled mobile robot that possesses dynamic object-tracking capability by using real-time image processing. Two motion control laws are proposed using Lyapunov's direct method and computed-torque method. Simulation results illustrate the effectiveness of the developed schemes. The overall experimental setup of the mobile robot developed in this paper is composed of a Windows based personal computer, Programmable Interface Controllers, a mobile robot, and an omni-directional vision system. Finally, the image-based real-time implementation experiments of the mobile robot demonstrate the feasibility and effectiveness of the proposed schemes.

***Key Words*:** Mobile Robot, Object Tracking, Motion Control, Programmable Interface Controller (PIC), Real-Time Implementation

1. Introduction

The problem addressed in the paper is the design of feedback controllers for a wheeled robot with non-holonomic constraints to track an object on the ground using visual feedback. The non-holonomic constraints restrict the admissible velocity space but not that of configuration. Because of these constraints, control design and analysis become substantially more involved. The control of non-holonomic wheeled mobile robot has been widely investigated in the literatures. Some researchers [1–8] designed the control on the basis of a kinematic state-space model derived from the constraints, but not taking the internal dynamics of the system into account.

Models that include dynamic effects are required for other purposes, for instance, using torques as control inputs and/or the inertia effect of the robot is not negligible. The approaches based on dynamic models of non-holonomic systems include the works in the literatures [9–16]. Campion et al. [9] and Bloch et al. [10] derived a full dynamical description of non-holonomic mechanical systems and showed a suitable change of coordinates allows for analysing globally the controllability and the state feedback stabilizability of the system. Sarkar et al. [12] presented a dynamic path-following algorithm for wheeled mobile robot by using a nonlinear feedback for input-output linearization and decoupling. Su and Stepanenko [11] developed a reduced dynamic model for simultaneous independent motion and force control of non-holonomic systems. They proposed a robust control law which is a smooth realization of sliding mode control. Shim et al. [13] proposed a variable structure control law, with which mobile robots converge to reference trajectories with bounded errors of position and velocity. Yang and Kim [15] developed a sliding mode control law by means of the computed-torque method for solving trajectory tracking problems of non-holonomic mobile robots. Lee [16] presented a switching control law, which, by utilizing the passivity property and energetic structure of the wheeled mobile robot, can ensure that the robot's

*Corresponding author. E-mail: ytwang@mail.tku.edu.tw

orientation converges to a target value, while driving the robot's (x, y)-trajectory to a desired position on the plane within a user-specified error-bound.

Visual feedback is a mature and inexpensive technology for servo control of non-holonomic wheeled mobile robots. There exist a lot of image-processing algorithms extracting a map of the environment from the data provided by a camera [17–20]. But the implementation of such sophisticated algorithms is quite complex. Ma et al. [7] formulated the tracking problem as one of directly controlling the shape of the curve in the image plane, instead of separately considering the estimation from the vision measurements and the design of control strategies. The practical implementation is, however, rather sophisticated, implying an extended Kalman filter to dynamically estimate the image parameters required for feedback control. Coulaud et al. [8] proposed a simple solution of the robot tracking problem, which avoids sophisticated image processing and control algorithms. Their practical implementation is straightforward, and can easily be achieved online. While the above works are mainly based on kinematic models of non-holonomic systems.

In this paper, we propose a novel control scheme for solving dynamic object-tracking problems of non-holonomic mobile robots using visual feedback. Dynamic models of mobile robots is used to describe their behaviors and, by means of a suitable change of coordinates, dynamics of mobile robots is linearized and two motion control laws based on Lyapunov's direct method and computed-torque method are applied for stabilizing the robots to a desired position and orientation. Mobile robots with the proposed control laws converge to a given desired position and orientation with asymptotic stability using real-time visual feedback and image processing. While the approach for object-tracking of non-holonomic systems via motion control was presented in the literatures [12,15], our approach has two contributions: First, in our approach, three-dimensional state variables of position and orientation are explicitly given as control outputs in two control stages, and the control inputs are designed to be applied motor torque. Second, experimental verification is shown. Few empirical studies on dynamic object-tracking of non-holonomic systems have been reported in the literatures, the proposed control laws are implemented on controlling a real non-holonomic wheeled mobile robot that has the dynamic model considered in this paper. Practical issues of visual servo control are addressed and results of the dynamic object-tracking control in the real world are shown.

This paper is organized as the following sections. In section 2, the dynamic equations of a two-wheeled autonomous robot are derived and the change of coordinates is applied to linearize the dynamics. The designs of robot motion controller based on the Laypunov's direct method and the computed-torque method are presented in section 3. In section 4, the proposed dynamic object-tracking behaviour of the non-holonomic mobile robot is described. In section 5, the experimental setup of mobile robot is depicted. And section 6 is the experimental results and discussions. We conclude the paper with some remarks in the last section.

2. Dynamics of a Wheeled Autonomous Robot

The dynamic equation of non-holonomic wheeled robot system is derived in this section, and the torque is selected as the control inputs which can be implemented easily in motion control design. A coordinate frame $x_m y_m$ is set on the chassis of the planar robot as shown in Figure 1. The robot has two driving wheels and one passive wheel. The robot system is fully described by a set of coordinates

$$(x \quad y \quad \phi \quad \beta \quad \theta_1 \quad \theta_2 \quad \theta_3)$$

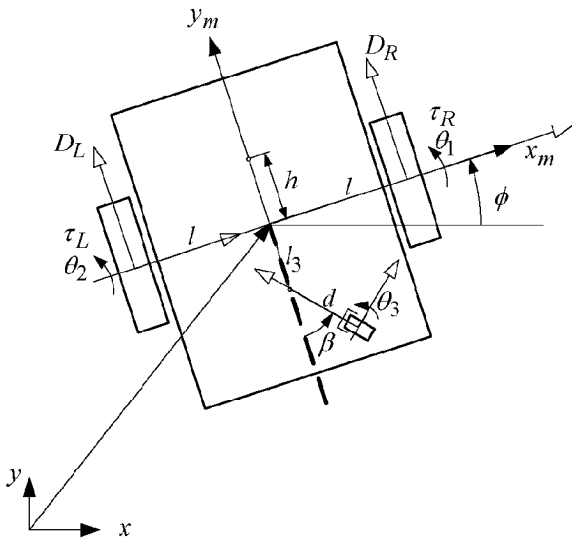

Figure 1. Mobile robot system.

Where *xy* are the axes of the fixed coordinate system; ϕ is the rotational angle between the robot frame and fixed coordinate; θ_i are the rotational angles of three robot wheels; β is the swinging angle of the passive wheel. The motions of three robot wheels in the direction being perpendicular to the wheel axis are constrained by three pure-rolling conditions,

$$-\dot{x}\sin\phi+\dot{y}\cos\phi+l\dot{\phi}-r\dot{\theta}_1=0 \tag{1a}$$

$$\dot{x}\sin\phi-\dot{y}\cos\phi+l\dot{\phi}+r\dot{\theta}_2=0 \tag{1b}$$

$$-\dot{x}\sin(\phi+\beta)+\dot{y}\cos(\phi+\beta)-l_3\dot{\phi}\sin\beta+r_3\dot{\theta}_3=0 \tag{1c}$$

where l is the length from the wheel to the centre of the robot chassis; l_3 is the length from the pivot of the passive wheel to the centre of the robot chassis. The motions of three robot wheels in lateral direction are constrained by three no-slipping conditions,

$$\dot{x}\cos\phi+\dot{y}\sin\phi=0 \tag{2a}$$

$$-\dot{x}\cos\phi-\dot{y}\sin\phi=0 \tag{2b}$$

$$\dot{x}\cos(\phi+\beta)+\dot{y}\sin(\phi+\beta)+(d+l_3\cos\beta)\dot{\phi}+d\dot{\beta}=0 \tag{2c}$$

Since the passive wheel is unpowered, θ_3 in Equation (1c) is free to rotate according to the robot motion. Meanwhile, any lateral motion of the passive wheel in Equation (2c) is balanced by the free rotational angle β. Therefore, Equations (1c) and (2c) do not constrain the motion of the robot. Therefore, the constraint equations (1a) and (1b) are the pure-rolling conditions of right and left wheels of the robot,

$$\begin{bmatrix}\omega_R\\ \omega_L\end{bmatrix}=\frac{1}{r}\begin{bmatrix}-\sin\phi & \cos\phi & l\\ -\sin\phi & \cos\phi & -l\end{bmatrix}\begin{bmatrix}\dot{x}\\ \dot{y}\\ \dot{\phi}\end{bmatrix} \tag{3}$$

where $\omega_R=\dot{\theta}_1$ and $\omega_L=\dot{\theta}_2$. The non-slipping constraint equations (2a) and (2b) are dependent and can be expressed as one single equation

$$\begin{bmatrix}\cos\phi & \sin\phi & 0\end{bmatrix}\begin{bmatrix}\dot{x}\\ \dot{y}\\ \dot{\phi}\end{bmatrix}=\boldsymbol{A}(\boldsymbol{q})^T\dot{\boldsymbol{q}}=0 \tag{4}$$

According to the integrability requirements of perfect differentials [21,22], Equation (4) is a non-holonomic constraint.

The dynamic equation of the robot can be derived by using the Lagrange formulation [21]:

$$\frac{d}{dt}\left(\frac{\partial \boldsymbol{L}}{\partial \dot{\boldsymbol{q}}}\right)-\frac{\partial \boldsymbol{L}}{\partial \boldsymbol{q}}=\boldsymbol{A}(\boldsymbol{q})\boldsymbol{\lambda}+\boldsymbol{B}(\boldsymbol{q})\boldsymbol{u} \tag{5}$$

where λ is the vector of Lagrange multiplier; $\boldsymbol{A}(\boldsymbol{q})\lambda$ is the vector of the generalized forces, which are applied on the system in order to satisfy the kinematic constraints; $\boldsymbol{B}(\boldsymbol{q})\boldsymbol{u}$ indicate the generalized forces, which are constructed by external forces and torques applied on the system by the actuators; $\boldsymbol{L}$ is the Lagrangian of the system. For the robot in planar motion as shown in Figure 1, it has

$$\boldsymbol{L}(\boldsymbol{q},\dot{\boldsymbol{q}})=\frac{1}{2}\dot{\boldsymbol{q}}^T\boldsymbol{M}(\boldsymbol{q})\dot{\boldsymbol{q}}$$

$$\boldsymbol{M}(\boldsymbol{q})=\begin{bmatrix}M & 0 & 0\\ 0 & M & 0\\ 0 & 0 & I_0\end{bmatrix}$$

Where $\boldsymbol{M}(\boldsymbol{q})$ is the matrix of mass and inertia.; M and I_0 are the mass and inertia of the robot system about the origin of robot coordinate, respectively. Substitute the Lagrangian into Equation (5), and have

$$\boldsymbol{M}(\boldsymbol{q})\ddot{\boldsymbol{q}}+\boldsymbol{C}(\boldsymbol{q},\dot{\boldsymbol{q}})\dot{\boldsymbol{q}}=\boldsymbol{A}(\boldsymbol{q})\lambda+\boldsymbol{B}(\boldsymbol{q})\boldsymbol{u} \tag{6}$$

$\boldsymbol{C}(\boldsymbol{q},\dot{\boldsymbol{q}})$ in left-hand side of the equation contains the nonlinear terms of the system and for planar robot is expressed as

$$\boldsymbol{C}(\boldsymbol{q},\dot{\boldsymbol{q}})\equiv\frac{d\boldsymbol{M}(\boldsymbol{q})}{dt}-\frac{1}{2}\frac{\partial}{\partial \boldsymbol{q}}[\dot{\boldsymbol{q}}^T\boldsymbol{M}(\boldsymbol{q})]=\boldsymbol{0}$$

For the planar robot, the external torque applied by the right and left wheels is

$$\boldsymbol{B}(\boldsymbol{q})\boldsymbol{u}=\begin{bmatrix}-\sin\phi & -\sin\phi\\ \cos\phi & \cos\phi\\ l & -l\end{bmatrix}\begin{bmatrix}D_R\\ D_L\end{bmatrix}$$

D_R and D_L are the driving forces of the right and left

wheels, respectively. The robot system equation (6) are derived as

$$M\ddot{x} = \lambda\cos\phi - (D_R + D_L)\sin\phi$$

$$M\ddot{y} = \lambda\sin\phi + (D_R + D_L)\cos\phi$$

$$I_0\ddot{\phi} = l(D_R - D_L)$$

The Dynamic equation (6) and the kinematic constraint equations (3) and (4) fully describe the robot system. Unfortunately, the Lagrange multiplier λ in Equation (6) can not be measured and controlled by the control system. The concept of null space is utilized to eliminate the Lagrange multiplier in the equations. The null space $\boldsymbol{S}(\boldsymbol{q})$ of $\boldsymbol{A}(\boldsymbol{q})$ are determined by solving the inner-production equation

$$\boldsymbol{A}^T(\boldsymbol{q})\boldsymbol{S}(\boldsymbol{q}) = 0 \tag{7}$$

The null space of $\boldsymbol{A}(\boldsymbol{q})$ is determined as

$$\boldsymbol{S}(\boldsymbol{q}) = \begin{bmatrix} -\sin\phi & 0 \\ \cos\phi & 0 \\ 0 & 1 \end{bmatrix}$$

Multiplying both sides of Equation (6) by $\boldsymbol{S}(\boldsymbol{q})$ to eliminate the Lagrange multiplier,

$$\boldsymbol{S}^T(\boldsymbol{q})[\boldsymbol{M}(\boldsymbol{q})\ddot{\boldsymbol{q}} + \boldsymbol{C}(\boldsymbol{q},\dot{\boldsymbol{q}})\dot{\boldsymbol{q}}] = \boldsymbol{S}^T(\boldsymbol{q})\boldsymbol{B}(\boldsymbol{q})\boldsymbol{u} \tag{8}$$

The non-holonomic equation (4) and Equation (7) imply that

$$\dot{\boldsymbol{q}} = \boldsymbol{S}(\boldsymbol{q})\boldsymbol{\eta}(\boldsymbol{q},\dot{\boldsymbol{q}}) \tag{9}$$

Where η are the variables in the null space of $\boldsymbol{A}(\boldsymbol{q})$ and chosen to be new state variables of the system. The new state variables are calculated by using Equation (9),

$$\eta_1 = -\dot{x}\sin\phi + \dot{y}\cos\phi$$

$$\eta_2 = \dot{\phi}$$

Substituting Equation (9) and its first time-derivative into Equation (8), it has

$$\boldsymbol{S}^T(\boldsymbol{q})\boldsymbol{M}(\boldsymbol{q})\boldsymbol{S}(\boldsymbol{q})\dot{\boldsymbol{\eta}} = \boldsymbol{S}^T(\boldsymbol{q})[-\boldsymbol{M}(\boldsymbol{q})\boldsymbol{\Delta}(\boldsymbol{q})\boldsymbol{\eta} - \boldsymbol{C}(\boldsymbol{q},\dot{\boldsymbol{q}})\boldsymbol{S}(\boldsymbol{q})\boldsymbol{\eta} + \boldsymbol{B}(\boldsymbol{q})\boldsymbol{u}]$$

Where $\Delta(\boldsymbol{q}) = d(S(q)) / dt$; Utilize the change of coordinate by applying the method of state feedback linearization [23], by defining the input as

$$\boldsymbol{B}(\boldsymbol{q})\boldsymbol{u} = \boldsymbol{M}(\boldsymbol{q})\boldsymbol{S}(\boldsymbol{q})\boldsymbol{v} + \boldsymbol{M}(\boldsymbol{q})\boldsymbol{\Delta}(\boldsymbol{q})\boldsymbol{\eta} + \boldsymbol{C}(\boldsymbol{q},\dot{\boldsymbol{q}})\boldsymbol{S}(\boldsymbol{q})\boldsymbol{\eta}$$

By applying the concept of null space and the change of coordinate, the new state equation for the planar robot is derived as

$$M\dot{\eta}_1 = D_R + D_L$$

$$I_0\dot{\eta}_2 = l(D_R - D_L)$$

Rearrange and obtain

$$\dot{\boldsymbol{\eta}}(\boldsymbol{q}) = \boldsymbol{v}(\boldsymbol{\eta},\boldsymbol{q}) = \begin{bmatrix} \frac{1}{M} & \frac{1}{M} \\ \frac{l}{I_0} & \frac{-l}{I_0} \end{bmatrix}\begin{bmatrix} D_R \\ D_L \end{bmatrix} \tag{10}$$

where $\boldsymbol{v}$ is the new input vector. Equation (10) completely describes the dynamics of the robot system and complies with the constraint equation.

In this research, the external torques is represented by the driving torques of the motor. As shown in Figure 2, the dynamic equations of right and left wheel are expressed as

$$I_w\dot{\omega}_R = \tau_R - rD_R - c\omega_R \tag{11a}$$

$$I_w\dot{\omega}_L = \tau_L - rD_L - c\omega_L \tag{11b}$$

Where I_w is the inertia of the wheel system; τ_R and τ_L are

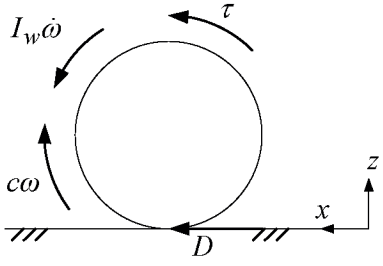

Figure 2. The wheel system.

the applied torques of the right and left motors, respectively; c is the coefficient of viscous friction; r is the radius of the wheel. From the pure-rolling conditions of right and left wheels and Equation (9), it has

$$\begin{bmatrix} \omega_R \\ \omega_L \end{bmatrix} = \frac{1}{r}\begin{bmatrix} 1 & l \\ 1 & -l \end{bmatrix}\begin{bmatrix} \eta_1 \\ \eta_2 \end{bmatrix} \tag{12}$$

Substitute Equation (12) and its first time-derivative into Equations (10) and (11), it can be obtained the new state equation of the robot system

$$\boldsymbol{M}'\dot{\boldsymbol{\eta}} + \boldsymbol{C}'\boldsymbol{\eta} = \boldsymbol{B}'\boldsymbol{\tau} \tag{13}$$

$$\boldsymbol{M}' = \begin{bmatrix} \dfrac{Mr^2 + 2I_w}{Mr} & 0 \\ 0 & \dfrac{I_0 r^2 + 2I_w l^2}{I_0 r} \end{bmatrix}$$

$$\boldsymbol{C}' = \begin{bmatrix} \dfrac{2c}{Mr} & 0 \\ 0 & \dfrac{2cl^2}{I_0 r} \end{bmatrix}, \quad \boldsymbol{B}' = \begin{bmatrix} \dfrac{1}{M} & \dfrac{1}{M} \\ \dfrac{l}{I_0} & \dfrac{-l}{I_0} \end{bmatrix}$$

The block diagram of the system is depicted as Figure 3. Note that, the input of the robot dynamic equation becomes the torque of the motor, which can be implemented easily in robot control scheme. Campion et al. [9] proved that with a smooth kinematic feedback control law:

$$\boldsymbol{w}(\boldsymbol{q}) = -\boldsymbol{S}^T(\boldsymbol{q})\boldsymbol{q}$$

The equilibrium point $\boldsymbol{q} = 0$ of the closed loop system is globally marginally stable. That is, the state $\boldsymbol{q}(t)$ is bounded as follows for all t: $|\boldsymbol{q}(t)| \le |\boldsymbol{q}(0)|$, and the state $\boldsymbol{q}(t)$ converges to the invariant set $U = \{\boldsymbol{q} | \boldsymbol{S}^T(\boldsymbol{q})\boldsymbol{q} = 0\}$. By the definition of the null space $\boldsymbol{S}(\boldsymbol{q})$, it has

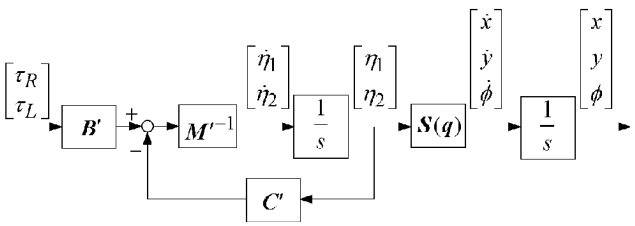

Figure 3. Block diagram of two-wheeled robot system.

$$-x\sin\phi + y\cos\phi = 0$$

$$\phi = 0$$

Therefore, the invariant set can be described as $y = \phi = 0$. Similarly, we can design a dynamic feedback control law, which is described in next section, providing the same globally marginal stability.

3. Design of Robot Motion Controllers

In this section, two robot motion control laws are designed based on Lyapunov's direct method and computed-torque method. By appropriate choices of output variables, the mobile robot with the designed control laws converge to a given desired position and orientation with asymptotic stability.

3.1 Design of Lyapunov Controller

The potential energy and kinetic energy of the robot system is selected as the Lyapunov function candidate,

$$V(\boldsymbol{\eta}, \tilde{\boldsymbol{q}}) = \frac{1}{2}\boldsymbol{\eta}^T\boldsymbol{M}'\boldsymbol{\eta} + \frac{1}{2}\tilde{\boldsymbol{q}}^T\boldsymbol{K}_P\tilde{\boldsymbol{q}}$$

The proportional control gain matrix $\boldsymbol{K_P}$ is symmetric and positive definite. $\tilde{\boldsymbol{q}} = \boldsymbol{q}_d - \boldsymbol{q}$ is defined as the position error, and $\boldsymbol{q}_d$ is the desired position. It has

$$\dot{V} = \boldsymbol{\eta}^T\boldsymbol{M}'\dot{\boldsymbol{\eta}} + \frac{1}{2}\boldsymbol{\eta}^T\dot{\boldsymbol{M}}'\boldsymbol{\eta} - \dot{\boldsymbol{q}}^T\boldsymbol{K}_P\tilde{\boldsymbol{q}}$$

$\boldsymbol{M}'\dot{\boldsymbol{\eta}}$ can be found by Equation (13), and $\dot{M}' = 0$. Therefore,

$$\dot{V} = -\boldsymbol{\eta}^T\boldsymbol{C}'\boldsymbol{\eta} + \boldsymbol{\eta}^T(\boldsymbol{B}'\boldsymbol{\tau} - \boldsymbol{S}^T\boldsymbol{K}_P\tilde{\boldsymbol{q}})$$

Similar to the kinematic feedback control law designed by Campion et al. [9], the dynamic control law is designed as

$$\boldsymbol{B}'\boldsymbol{\tau} = \boldsymbol{S}^T(\boldsymbol{K}_P\tilde{\boldsymbol{q}} - \boldsymbol{K}_D\dot{\boldsymbol{q}}) \tag{14}$$

The derivative control gain matrix $\boldsymbol{K_D}$ is symmetric and positive definite. Therefore,

$$\dot{V} = -\boldsymbol{\eta}^T\boldsymbol{C}'\boldsymbol{\eta} - \dot{\boldsymbol{q}}^T\boldsymbol{K}_D\dot{\boldsymbol{q}} \le 0$$

The block diagram of the motion controller based on Lyapunov's direct method is depicted as Figure 4. The simulation result of step response for the Lyapunov controller is shown in Figure 5. The figure depicts that the dynamic control system is globally marginally stable and the state $\boldsymbol{q}(t)$ converges to the invariant set $y = \phi = 0$, but x can only be stable in a range of the initial value.

3.2 Design of Computed-Torque Controller

In order to control the robot to desired location $[x\ y]^T$, the concept of computed-torque method [24] is utilized to design another motion controller. Choose the outputs to be $[\bar{x}\ \bar{y}]^T$, which point locates at the pivot of the third wheel as shown in Figure 1,

$$\begin{bmatrix}\bar{x}\\ \bar{y}\end{bmatrix} = \begin{bmatrix}x + l_3\sin\phi\\ y - l_3\cos\phi\end{bmatrix}$$

Hence, the time derivative of the outputs will be

$$\dot{\bar{x}} = \dot{x} + l_3\dot{\phi}\cos\phi = -\eta_1\sin\phi + l_3\eta_2\cos\phi$$

$$\dot{\bar{y}} = \dot{y} + l_3\dot{\phi}\sin\phi = \eta_1\cos\phi + l_3\eta_2\sin\phi$$

$$\ddot{\bar{x}} = -\eta_1\dot{\phi}\cos\phi - l_3\eta_2\dot{\phi}\sin\phi - v_1\sin\phi + l_3 v_2\cos\phi$$

$$\ddot{\bar{y}} = -\eta_1\dot{\phi}\sin\phi + l_3\eta_2\dot{\phi}\cos\phi + v_1\cos\phi + l_3 v_2\sin\phi$$

Written in matrix form

$$\ddot{\boldsymbol{q}} = \boldsymbol{C''}(\boldsymbol{q},\dot{\boldsymbol{q}})\eta + \boldsymbol{B''}\boldsymbol{v} \tag{14}$$

$$\mathbf{C''}(\mathbf{q},\dot{\mathbf{q}}) = \begin{bmatrix}-\dot{\phi}\cos\phi & -l_3\dot{\phi}\sin\phi\\ -\dot{\phi}\sin\phi & l_3\dot{\phi}\cos\phi\end{bmatrix}$$

$$\mathbf{B''} = \begin{bmatrix}-\sin\phi & l_3\cos\phi\\ \cos\phi & l_3\sin\phi\end{bmatrix}$$

Design the control input of the controller by using the computed-torque method

$$\boldsymbol{v} = \boldsymbol{B''}^{-1}(-\boldsymbol{C''}\eta + \ddot{\boldsymbol{q}}_d + \boldsymbol{K}_P\tilde{\boldsymbol{q}} + \boldsymbol{K}_D\dot{\tilde{\boldsymbol{q}}}) \tag{15}$$

$$\boldsymbol{B''}^{-1} = \begin{bmatrix}\sin\phi & -\cos\phi\\ -\frac{1}{l_3}\cos\phi & -\frac{1}{l_3}\sin\phi\end{bmatrix}$$

where $\boldsymbol{K_P}$ and $\boldsymbol{K_D}$ are the proportional and derivative gain matrices, respectively. From Equation (15), it can be seen that l_3 can not be zero. Substituting Equation (14) into Equation (15), it becomes

$$\ddot{\tilde{\boldsymbol{q}}} + \boldsymbol{K}_D\dot{\tilde{\boldsymbol{q}}} + \boldsymbol{K}_P\tilde{\boldsymbol{q}} = 0$$

The control torque $[\tau_R\ \tau_L]^T$ can be derived as

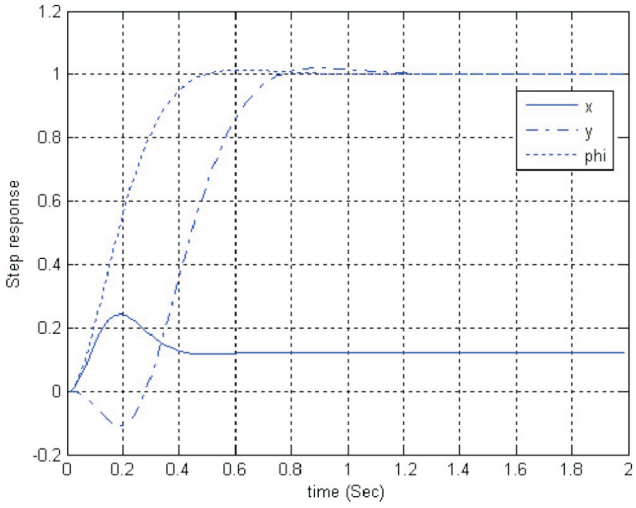

Figure 5. Step response of the Lyapunov controller.

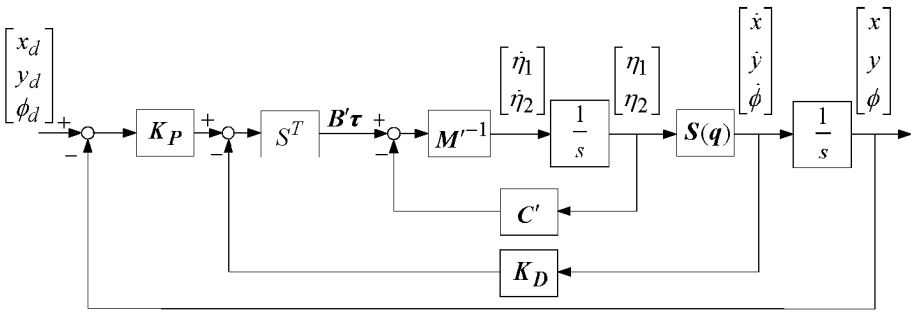

Figure 4. Block diagram of the Lyapunov controller.

$$\begin{bmatrix}\tau_R\\ \tau_L\end{bmatrix}=\begin{bmatrix}\frac{Mr}{2} & \frac{I_0 r}{2l}\\ \frac{Mr}{2} & -\frac{I_0 r}{2l}\end{bmatrix}\begin{bmatrix}v_1\\ v_2\end{bmatrix}+\frac{c}{r}\begin{bmatrix}-\sin\phi & \cos\phi & l\\ -\sin\phi & \cos\phi & -l\end{bmatrix}\begin{bmatrix}\dot{x}\\ \dot{y}\\ \dot{\phi}\end{bmatrix}$$
$$+\frac{I_w}{r}\begin{bmatrix}-\dot{\phi}\cos\phi & -\dot{\phi}\sin\phi & 0\\ -\dot{\phi}\cos\phi & -\dot{\phi}\sin\phi & 0\end{bmatrix}\begin{bmatrix}\dot{x}\\ \dot{y}\\ \dot{\phi}\end{bmatrix} \quad (16)$$
$$+\frac{I_w}{r}\begin{bmatrix}-\sin\phi & \cos\phi & l\\ -\sin\phi & \cos\phi & -l\end{bmatrix}\begin{bmatrix}\ddot{x}\\ \ddot{y}\\ \ddot{\phi}\end{bmatrix}$$

Or in matrix form

$$\boldsymbol{\tau} = \boldsymbol{rH'v} + \boldsymbol{f}(\boldsymbol{q},\dot{\boldsymbol{q}},\ddot{\boldsymbol{q}})$$

Note that,

$$\begin{bmatrix}\ddot{x}\\ \ddot{y}\\ \ddot{\phi}\end{bmatrix}=\begin{bmatrix}-\dot{\eta}_1\sin\phi-\eta_1\dot{\phi}\cos\phi\\ \dot{\eta}_1\cos\phi-\eta_1\dot{\phi}\sin\phi\\ \dot{\eta}_2\end{bmatrix}$$

The block diagram of the computed-torque controller is shown in Figure 6. The step response of the controller is shown as Figure 7. Since the control outputs are chosen to be the desired x and y locations, Figure 7 depicts that x and y can be achieved to the desired position with asymptotic stability. However, ϕ is hard to reach the desired angle.

4. Design of Dynamic Object-Tracking Behavior

The robot behaviour of dynamic object-tracking is planned using the proposed motion controllers. Before planning the object-tracking behaviour, we simulate the motion control using the proposed Lyapunov controller and computed-torque controller. As shown in Figures 8 and 9, the robot initially locates on eight different positions of a circle with radius of 10 m, and the desired output position is $[y\ x\ \phi]^T = [0m\ 0m\ 0rad]^T$. The results of motion control by the Lyapunov controller are shown in Figure 8. The figure depicts that the motion control can achieve the desired output in position y and orientation ϕ, while the desired position in x direction can not be stably controlled. On the other hand, Figure 9 depicts the results of motion control from eight positions of a circle by using the computed-torque controller. The results depict that the motion control can achieve the desired output in

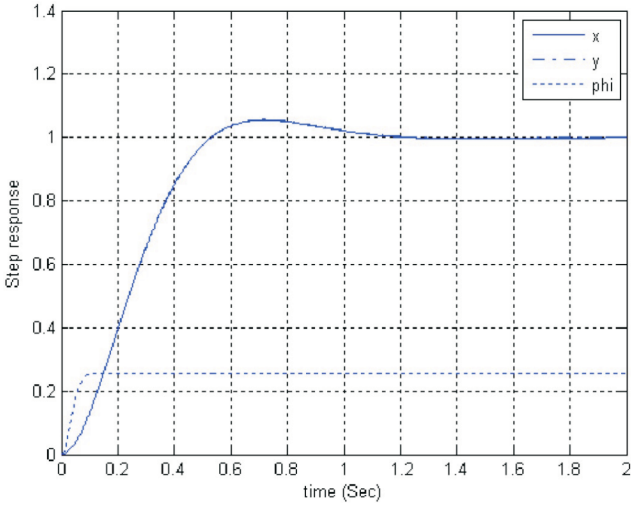

Figure 7. Step response of computed-torque controller.

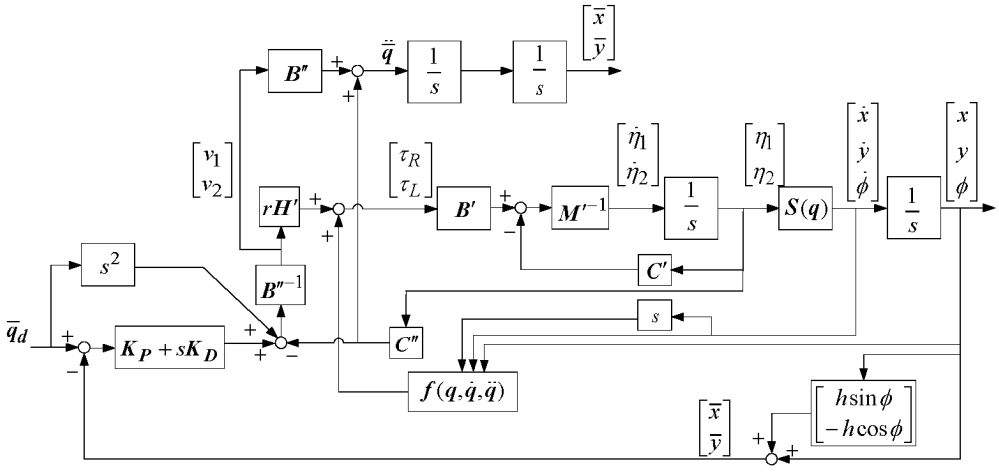

Figure 6. Block diagram of the computed-torque controller.

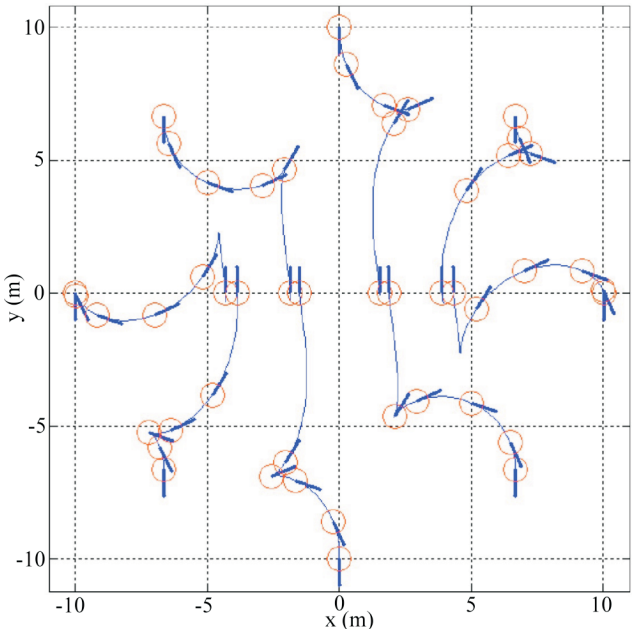

Figure 8. Motion control by using the Lyapunov controller.

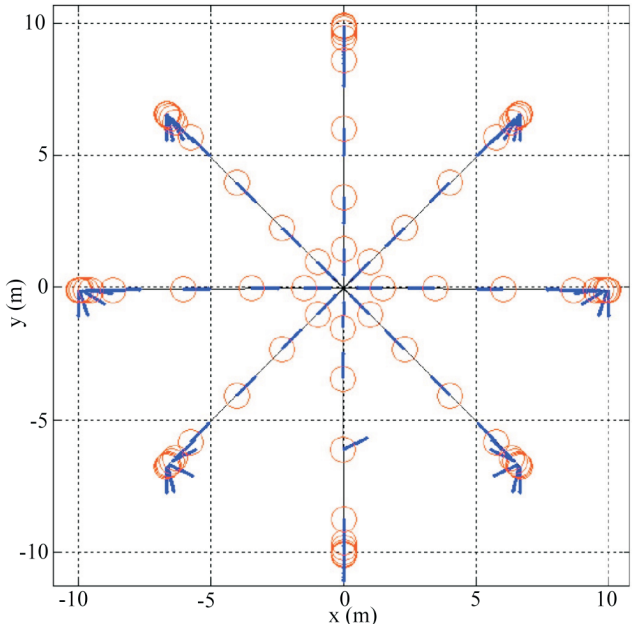

Figure 9. Motion control by using the computed-torque controller.

position x and y, but not in orientation ϕ.

We propose to plan the dynamic object-tracking behaviour of the robot by using the Lyapunov controller and the computed-torque controller in two stages. As depicted in Figure 10, the tracking behaviour is composed of two motion controllers in these two stages. In stage 1, the robot moves from the initial position (x_0, y_0) to the

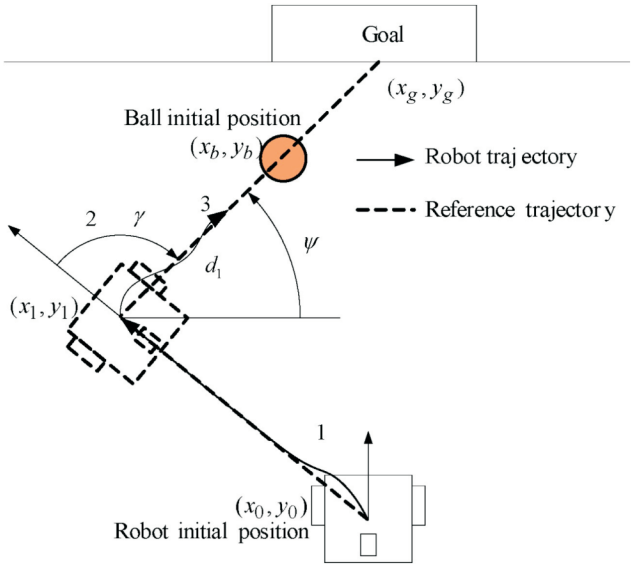

Figure 10. Robot object-tracking behaviour.

candidate point (x_1, y_1) by using the computed-torque controller. In stage 2, the robot turns with an angle γ to reach the angle ψ by using the Lyapunov controller, and then push the ball to the goal by using the computed-torque controller again. If the orientation of the robot is deviated from the desired direction by a preset threshold value, the Lyapunov controller will be recalled to convert the deviation.

5. Wheeled Mobile Robot System

In this section, we present the design and implement of the non-holonomic wheeled robot. The experimental setup of the wheeled robot system, as shown in Figure 11, is composed of a Windows based personal computer (PC), Programmable Interface Controllers (PIC), a mobile robot, and an omni-directional vision system. The omni-directional vision is utilized to capture the image surrounding the robot, as shown in Figure 12, for calculating the distance from an object to the robot [25]. The architecture of the control system is shown in Figure 13. All the parameter values of the robot system are experimentally obtained and depicted [26]. A PC is in charge of implementing the algorithms including feature recognition and tracking, Simultaneous Localization and Mapping (SLAM), and path planning and obstacle avoidance. Motion and current control laws are implemented in PIC microcontrollers for the driving motors. For example, control of one-axis motor is depicted in Figure 14. In the

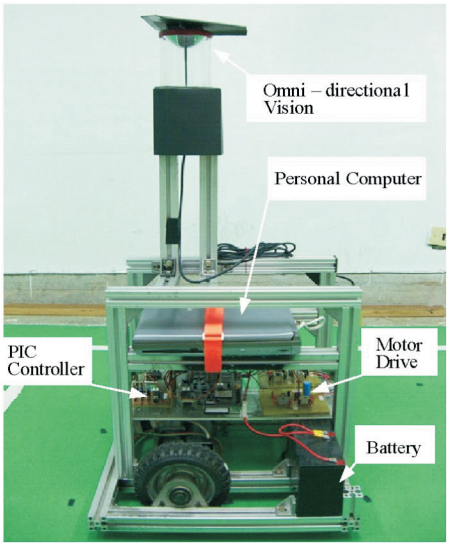

Figure 11. Wheeled mobile robot.

dynamic control of the robot, motor driving torques are chosen as the input commands which are implemented by Pulse Width Modulation (PWM) signals and sent to the motor drive circuits.

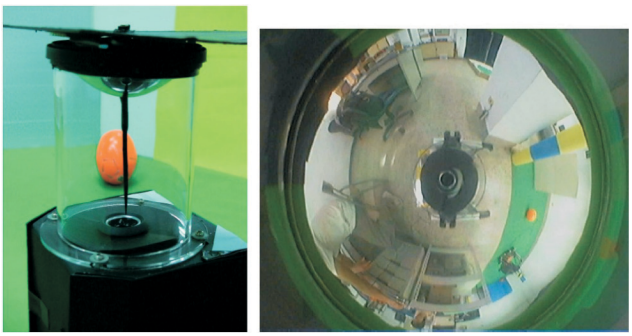

Figure 12. Omni-directional vision system.

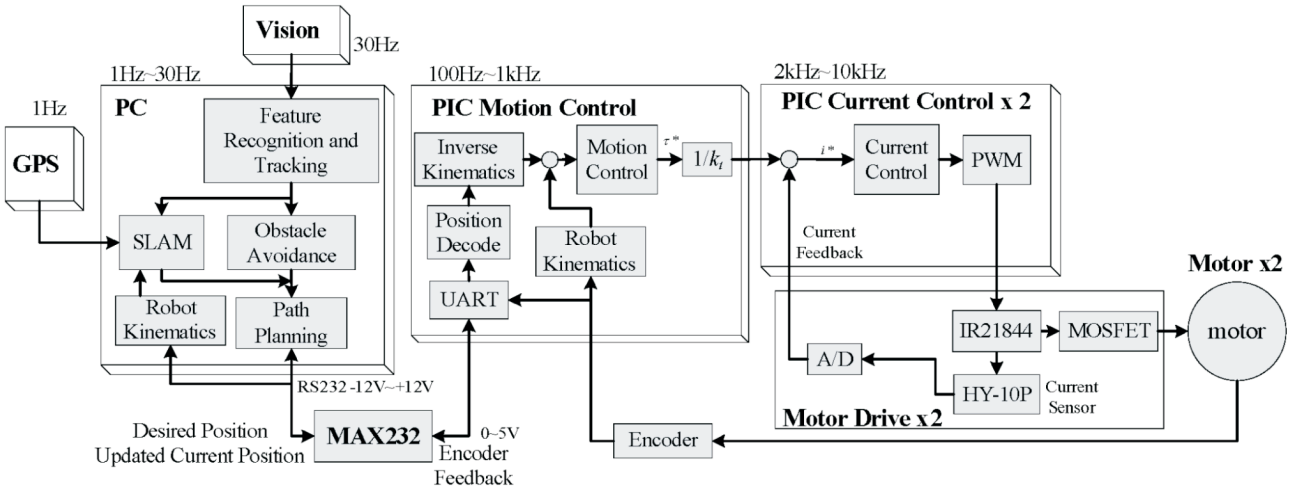

Figure 13. Architecture of the robot system.

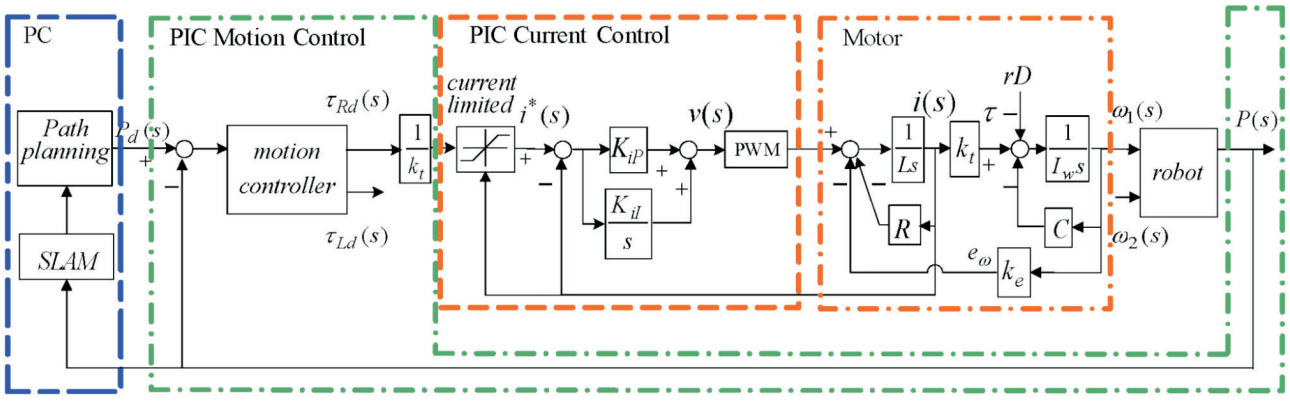

Figure 14. Block diagram of motion and current control for the robot system.

6. Experimental Results

The experimental setup of wheeled mobile robot is tested on the ground to track a ball dynamically. Two dynamic motion controls are combined to form the robot object-tracking behaviour. The results are shown in Figures 15 and 16. Figure 15 depicts the continuous tracking motions of the robot. Figure 16 depicts the trajectory of the ball in polar coordinates. Initially, the ball located in the direction of $\phi = 122°$ and a distance of 85 image pixels. The robot turns firstly, and then approaches to the ball. Finally, the ball is located between the robot and the goal.

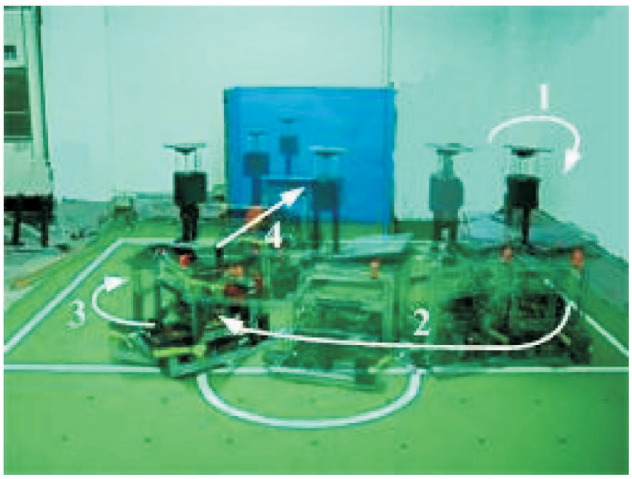

Figure 15. Continuous tracking motions of the robot.

7. Conclusion Remarks

In this paper, we plan a dynamic object-tracking behavior for a non-holonomic mobile robot using two developed motion control laws. The mobile robot with the proposed control laws converge to a given reference trajectory with asymptotic stability using real-time visual feedback and image processing. Two major contributions by this research include: The state variables of position and orientation are explicitly given as control outputs in two control stages, and the control inputs are planned by using motor driving torque which is easily implemented in mechatronics system. Meanwhile, the proposed control laws are implemented on controlling a real non-holonomic wheeled mobile robot using a personal computer and PIC microcontrollers. The image-based real-time implementation experiments of the mobile robot demonstrate the feasibility and effectiveness of the proposed schemes.

Acknowledgement

This work was supported by the National Science Council in Taiwan under grant no. NSC95-2221-E-032-055-MY2 to Y. T. Wang.

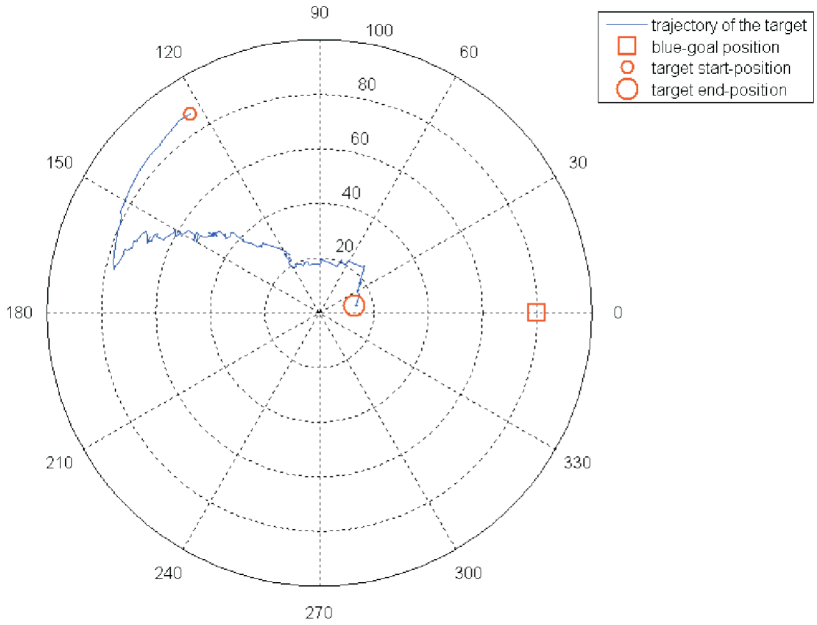

Figure 16. The trajectory of the ball in polar coordinates.

References

[1] Laumond, J. P., "Feasible Trajectories for Mobile Robots with Kinematic and Environment Constraints," *Proceedings of International Conference on Intelligent Autonomous Systems*, pp. 346–354 (1986).

[2] Barraquand, J. and Latombe, J. C., "On Nonholonomic Mobile Robots and Optimal Maneuvering," *Proceedings of the IEEE International Symposium on Intelligent Control*, pp. 340–347 (1989).

[3] Sordalen, O. J. and Canudas de Wit, C., "Exponential Control Law for a Mobile Robot: Extension to Path Following," *IEEE Transactions on Robotics and Automation*, Vol. 9, pp. 837–842 (1993).

[4] Astolfi, A., "Discontinuous Control of Nonholonomic Systems," *Systems and Control Letters*, Vol. 27, pp. 37–45 (1996).

[5] Fierro, R. and Lewis, F. L., "Control of a Nonholonomic Mobile Robot: Backstepping Kinematics into Dynamics," *Journal of Robotic Systems*, Vol. 14, pp. 149–163 (1997).

[6] Hespanha, J. P. and Morse, A. S., "Stabilization of Nonholonomic Integrators via Logic-Based Switching," *Automatica*, Vol. 35, pp. 385–393 (1999).

[7] Ma, Y., Kosecka, J. and Sastry, S. S., "Vision Guided Navigation for a Nonholonomic Mobile Robot," *IEEE Transactions on Robotics and Automation*, Vol. 15, pp. 521–536 (1999).

[8] Coulaud, J.-B., Campion, G., Bastin, G. and De Wan, M., "Stability Analysis of a Vision-Based Control Design for an Autonomous Mobile Robot," *IEEE Transactions on Robotics*, Vol. 22, pp. 1062–1069 (2006).

[9] Campion, G., d'Andrea-Novel, B. and Bastin, G., "Controllability and State Feedback Stability of Nonholonomic Mechanical Systems," In *Advanced Robot Control, Proceedings of International Workshop in Adaptive and Nonlinear Control: Issues in Robotics*, pp. 106–124, Grenoble (1990).

[10] Bloch, A. M., Reyhanoglu, M. and McClamroch, N. H., "Control and Stabilization of Nonholonomic Dynamic Systems," *IEEE Transactions on Automatic Control*, Vol. 37, pp. 1746–1757 (1992).

[11] Su, C. Y. and Stepanenko, Y., "Adaptive Control of a Class of Nonlinear Systems with Fuzzy Logic," *IEEE Transactions on Fuzzy Systems*, Vol. 2 pp. 285–294 (1994).

[12] Sarkar, N., Yun, X. and Kumar, V., "Control of Mechanical Systems with Rolling Constraints: Application to Dynamic Control of Mobile Robots," *The International Journal of Robotics Research*, Vol. 13, pp. 55–69 (1994).

[13] Shim, H.-S., Kim, J.-H. and Koh, K., "Variable Structure Control of Nonholonomic Wheeled Mobile Robots," in *Proceeding IEEE International Conference on Robotics and Automation*, pp. 1694–1699 (1995).

[14] Kolmanovsky, I., Reyhanoglu, M. and McClamroch, N. H., "Switched Mode Feedback Control Laws for Nonholonomic Systems in Extended Power Form," *Systems and Control Letters*, Vol. 27, pp. 29–36 (1996).

[15] Yang, J. M. and Kim, J. H., "Sliding Mode Control for Trajectory Tracking of Nonholonomic Wheeled Mobile Robots," *IEEE Transactions on Robotics and Automation*, Vol. 15, pp. 578–587 (1999).

[16] Lee, D., "Passivity-Based Switching Control for Stabilization of Wheeled Mobile Robots," *Proceedings of Robotics Science and Systems Conference* (2007).

[17] Broggi, A., Bertozzi, M., Fascioli, A. and Conte, G., *Automatic Vehicle Guidance: The Experience of the Argo Autonomous Vehicle*, World Scientific (1999).

[18] Corke, P. I., Symeonidis, D. and Usher, K., "Tracking Road Edges in the Panospheric Image Plane," *Proceedings IEEE/RSJ International Conference on Intelligent Robots and System*, pp. 1330–1335 (2003).

[19] Pomerleau, D. and Jochem, T., "Rapidly Adapting Machine Vision for Automated Vehicle Steering," *IEEE Expert*, Vol. 11, pp. 19–27 (1996).

[20] Taylor, C. J., Kosecka̋, J., Blasi, R. and Malik, J., "A Comparative Study of Vision-Based Lateral Control Strategies for Autonomous Highway Driving," *International Journal of Robotics Research*, Vol. 18, pp. 442–453 (1999).

[21] D'Souza, A. F. and Garg, V. K., *Advanced Dynamics: Modeling and Analysis*, Prentice-Hall (1984).

[22] Campion, G., Bastin, G. and D'Andrea-Novel, B., "Structural Properties and Classification of Kinematic and Dynamic Models of Wheeled Mobile Robots," *IEEE Transactions on Robotics and Automation*, Vol. 12, pp. 47–62 (1996).

[23] Slotine, J.-J. E. and Li, W., *Applied Nonlinear Control*, Prentice-Hall (1991).

[24] d'Andrea-Novel, B., Bastin, G. and Campion, G.,

"Modelling and Control of Non Holonomic Wheeled Mobile Robots," *Proceedings of IEEE International Conference of Robotics and Automation*, pp. 1130–1135, Sacramento, CA (1991).

[25] Bunschoten, R. and Kröse, B., "Robust Scene Reconstruction from an Omnidirectional Vision System," *IEEE Transactions on Robotics and Automation*, Vol. 19, pp. 351–357 (2003).

[26] Hsieh, J.-J., *Self-Localization and Motion Control of an Autonomous Campus-Guiding Robot*, Master Thesis, Department of Mechanical and Electro-Mechanical Engineering, Tamkang University (in Chinese) (2008).

Manuscript Received: Feb. 15, 2009
Accepted: Mar. 3, 2009